Supporting Information

Trokter et al. 10.1073/pnas.1210573110

SI Materials and Methods

Cloning and Expression of Dynein Heavy-Chain Constructs and Associated Subunits. Full-length human cytoplasmic dynein 1 heavy chain 1 (DYNC1H1; UniProtKB accession no. Q14204) cDNA encoding 4,646 aa was generated by producing three fragments that were subsequently combined and inserted into a modified baculoviral expression vector with inserted mGFP (pFastBacHT-mGFP), generating His_6-mGFP-CDHC (CDHC).

In detail, three fragments covering the entire full-length CDHC cDNA were first generated. A cDNA encoding the 3′ fragment (encoding amino acids 1947–4646 of the protein) was obtained from the cDNA clone DKFZp686G1167 (ImaGenes; GenBank accession no. AL833600.1) and amplified by PCR. Mutations present in the cDNA clone (R3339H, F3354L, K3774X, L3863P) were reverted to the National Center for Biotechnology Information (NCBI) reference sequence NM_001376 using site-directed mutagenesis (Stratagene). The 5′ fragment (encoding amino acids 1–1190) and the central fragment (encoding amino acids 1187–1970) were generated by RT-PCR of mRNA isolated from HeLa cells using gene-specific primers. The amplified fragments were first cloned into PCR-XL-TOPO vector (Invitrogen). For the ligation of the 5′- and central cDNA fragment, an existing SacI restriction site was used. For the ligation of the central and the 3′ fragment, we introduced a SacII restriction site without changing the amino acid composition of the protein (at amino acid position 1969–1970). For the ligation of the 5′ end of the CDHC cDNA, a MluI site was introduced into the multiple cloning site (MCS) of pFastBacHTa, and for the ligation of the 3′ end, the existing SpeI site in MCS was used. A sequence encoding mGFP (the K221L mutation of eGFP) (1) was inserted before the MluI site in the modified pFastBacHTa, generating pFastBacHT-mGFP. Full-length CDHC was assembled and cloned into pFastBacHT-mGFP by simultaneous ligation of four fragments (three CDHC cDNA fragments and the vector), generating an expression vector encoding for His_6-mGFP-CDHC, with amino acids GGGYASGA linking mGFP and CDHC.

A sequence encoding the C-terminal 380-kDa dynein motor domain (1,303–4,646 aa) was amplified from His_6-mGFP-CDHC and cloned into the pFastBacHT-mGFP vector, generating His_6-mGFP-Dyn380kD, with amino acids GGGYASGGTGGAAA linking mGFP and Dyn380kD.

An artificial dimer of dynein motor domains was generated by fusing the sequence encoding for a kinesin-1 coiled coil to the 5′ end of the dynein motor domain. The coiled coil fragment (cc) (encoding kinesin-1, amino acids 337–414) was amplified from the human kinesin-1 heavy-chain full-length cDNA clone IRCMp5012D0817D from ImaGenes (UniProtKB accession no. P33176) and cloned into pFastBacHT-mGFP-Dyn380kD, generating His_6-mGFP-cc-Dyn380kD, with amino acids GGGYASGG linking mGFP and cc, and amino acids GSGGGAA linking cc and Dyn380kD.

The accessory subunits of the dynein complex were amplified from a first-strand cDNA library from human brain (Origene) by PCR using primers suitable to amplify any of the respective isoforms. We obtained sequences for human cytoplasmic dynein 1 IC1 isoform 2 (DYNC1I1; UniProtKB accession no. O14576-2; 628 aa), human cytoplasmic dynein 1 LIC2 (DYNC1LI2; UniProtKB accession no. O43237; 492 aa), human cytoplasmic dynein LC8 light chain 1 (DYNLL1; UniProtKB accession no. P63167; 89 aa), human dynein RB light chain 1 (DYNLRB1; UniProtKB accession no. Q9NP97; 96 aa), and human dynein Tctex1 light chain 1 (DYNLT1; UniProtKB accession no. P63172; 113 aa). All five subunits [IC1, LIC2, and the light chains (LC8, RB1, and Tctex1)] were cloned into a bacterial expression vector pETZt2, generating His_6-Ztag proteins, containing a tobacco etch virus (TEV) protease cleavage site between Z tag and the protein. IC1 was additionally cloned into a baculoviral expression vector pFastBacET (version of pFastBac 1 with modified MCS), generating a construct without additional tags.

The accuracy of each cloned sequence described above was confirmed by sequencing.

pFastBac vectors were used to generate recombinant baculoviruses for insect cell expression, essentially as described (2). All of the baculoviruses were titered and used in a dilution that allows the infected Sf21 insect cells to divide once before cell-proliferation arrest (low multiplicity of infection). His_6-mGFP-CDHC and IC1 were expressed for 60 h after proliferation arrest, whereas His_6-mGFP-Dyn380kD and His_6-mGFP-cc-Dyn380kD were expressed 72 h after the arrest. After the expression, the cells were harvested and frozen in liquid nitrogen.

Protein Purification. ***Dynein heavy-chain constructs.*** Cells expressing either full-length CDHC or truncated dynein construct (His_6-mGFP-CDHC, His_6-mGFP-Dyn380kD, or His_6-mGFP-cc-Dyn380kD) were lysed in ice-cold lysis buffer A [50 mM Hepes, 250 mM potassium acetate (KOAc), 2 mM $MgSO_4$, 10% glycerol (vol/vol), 0.2 mM Mg-ATP, 10 mM β-mercaptoethanol, 30 mM imidazole (pH 7.4), protease inhibitors (Complete EDTA-free; Roche)] supplemented with 0.5 mM EDTA using a glass homogenizer (Fisher Scientific). The lysate was clarified by centrifugation at 250,000 × *g* for 30 min at 4 °C and applied to 1-mL HisTrap HP column (IMAC; GE Healthcare) equilibrated in lysis buffer A. The column was then washed extensively with lysis buffer A, and the protein was eluted with elution buffer A [30 mM Hepes, 150 mM KOAc, 2 mM $MgSO_4$, 0.25 mM EDTA, 10% glycerol (vol/vol), 0.2 mM Mg-ATP, 10 mM β-mercaptoethanol, 500 mM imidazole (pH 7.4), protease inhibitors] using a linear gradient of 10 mL. Dynein-containing fractions were pooled, and the buffer was exchanged into gel-filtration buffer A [30 mM Hepes, 150 mM KOAc, 2 mM $MgSO_4$, 0.5 mM EGTA, 10% glycerol (vol/vol), 0.1 mM Mg-ATP, 10 mM β-mercaptoethanol (pH 7.2)] using a PD10 desalting column (GE Healthcare). The protein was gel-filtered using a Superose 6 10/300 GL column (GE Healthcare) equilibrated in gel-filtration buffer A and concentrated. [The absorbance values at 280 and 488 nm of mGFP-labeled dynein constructs indicated that there was roughly one mGFP per each dynein monomer. There was also a significant fraction of His_6-mGFP in the eluate that was well separated from the dynein construct (Fig. S1*B*, *Inset*) and was probably a consequence of prematurely terminated translation.] After centrifugation at 100,000 × *g* for 10 min at 4 °C, the protein concentration was determined by measuring the absorbance at 280 nm and using a molar extinction coefficient calculated from its primary sequence (Expasy; http://expasy.org/tools/protparam.html). The concentration was confirmed by Bradford using BSA as a standard. Proteins were supplemented with glycerol to a final concentration of 20% (vol/vol), flash-frozen in small aliquots, and stored in liquid nitrogen. The final yields of purified Dyn380kD and cc-Dyn380kD were typically ∼2 mg from 500 mL of Sf21 cell culture, with a final concentration up to ∼1 mg/mL. In contrast, purified CDHC could not be concentrated beyond ∼0.03 mg/mL.

Mass spectroscopic analysis of the artificially dimerized dynein confirmed that the entire amino acid sequence of this construct

could be detected (with an amino acid coverage of the sequence of 66%), demonstrating that the purified protein was intact.

For the analysis of hydrodynamic properties and oligomerization state under higher-ionic-strength conditions (in Fig. S4), dynein constructs were purified using purification buffers of higher ionic strength: lysis buffer B [50 mM KH_2PO_4, 500 mM KCl, 2 mM $MgCl_2$, 10% glycerol (vol/vol), 0.2 mM Mg-ATP, 10 mM β-mercaptoethanol, 30 mM imidazole (pH 7.4), protease inhibitors], elution buffer B [50 mM KH_2PO_4, 500 mM KCl, 2 mM $MgCl_2$, 0.25 mM EDTA, 10% glycerol (vol/vol), 0.2 mM Mg-ATP, 10 mM β-mercaptoethanol, 500 mM imidazole (pH 7.4), protease inhibitors], and gel-filtration buffer B [20 mM KH_2PO_4, 250 mM KCl, 2 mM $MgCl_2$, 0.5 mM EGTA, 10% glycerol (vol/vol), 0.1 mM Mg-ATP, 10 mM β-mercaptoethanol (pH 7.2)].

Heavy-chain–associated subunits. pETZt2 constructs (IC1, LIC2, LC8, RB1, and Tctex1) were used to transform *E. coli* BL21 RIL cells, and the culture was grown from a single clone to an OD_{600} of 0.6. Protein expression was induced by adding 0.1 mM isopropylthio-β-galactoside (IPTG), and the culture was incubated overnight at 18 °C shaking at 200 rpm. Cells were harvested and lysed in lysis buffer C [50 mM NaH_2PO_4, 300 mM KCl, 2 mM $MgCl_2$, 1 mM β-mercaptoethanol, 5 mM imidazole (pH 7.5)] supplemented with protease inhibitors (Complete EDTA-free; Roche) using a high-pressure homogenizer (Emulsiflex C-5; Avestin). The cell lysate was clarified by centrifugation at 250,000 × *g* for 30 min at 4 °C and applied to a 5-mL HiTrap chelating HP column (GE Healthcare) loaded with cobalt ions and equilibrated with lysis buffer C. The column was then washed extensively with lysis buffer C, and the protein was eluted with lysis buffer C supplemented with 350 mM imidazole. The eluted protein was dialyzed into lysis buffer C and incubated overnight at 4 °C with oligo-histidine–tagged TEV protease (1 mg of protease per 30 mg of substrate). Cleaved His_6-Z tag and the protease were removed by rebinding to a cobalt-charged HiTrap chelating HP column. The flow-through (containing cleaved proteins) was concentrated and further purified by gel filtration using a HiLoad 16/60 Superdex 200-pg column equilibrated in gel-filtration buffer C [20 mM NaH_2PO_4, 250 mM KCl, 2 mM $MgCl_2$, 5 mM β-mercaptoethanol (pH 7.2)]. The protein concentration was determined by Bradford using BSA as a standard. Proteins were supplemented with glycerol to a final concentration of 20% (vol/vol), flash-frozen, and stored in liquid nitrogen.

IC1 was the only accessory subunit that was insoluble after the cleavage of the solubility-enhancing tag (Z tag), probably because of misfolding in the absence of the heavy chain and/or light chains that it is usually interacting with.

Reconstitution of dynein complex. To assemble and purify the cytoplasmic dynein complex, consisting of CDHC, IC1, LIC2, and three light chains, we first preassembled a ternary complex. The heavy chain and IC1 (both expressed in insect cells) were not purified before complex assembly, because in contrast to the other subunits, they were insoluble when purified individually. Four grams of cells expressing His_6-mGFP-CDHC (~1–2 mg expressed CDHC; 2–3.5 nmol) and 1 g of cells expressing IC1 (~5–10 mg expressed IC1; 70–140 nmol) were resuspended in ice-cold lysis buffer A supplemented with 0.5 mM EDTA. The cell suspensions were mixed and lysed using a glass homogenizer. Purified LIC2 (2 mg; ~35 nmol) was added to the lysate, and this mixture was centrifuged at 250,000 × *g* for 30 min at 4 °C. Clarified lysate was applied to 1-mL HisTrap HP column equilibrated in lysis buffer A. The column was then washed extensively with lysis buffer A, the protein was eluted with elution buffer A using a linear gradient of 10 mL, and dynein-containing fractions were pooled. This first purification step removed excess IC1 and LIC2, and the obtained ternary complex is the minimal complex showing good solubility (Table 1). Then, 150 μg (~10 nmol) of each purified light chain (LC8, RB1, and Tctex1) were added to the eluate. The buffer of this protein mixture was immediately exchanged into gel-filtration buffer A using a PD10 desalting column, and the sample was gel-filtered using a Superose 6 10/300 GL column equilibrated in gel-filtration buffer A. The fractions following the void-volume peak of the column, as indicated in Fig. 1*E*, were collected. The solution was concentrated and centrifuged at 100,000 × *g* for 10 min at 4 °C. The extinction coefficient and molecular mass that were used for calculation of the concentration of the complex in the supernatant were obtained by adding the molar extinction coefficients and molecular masses, respectively, of the six subunits calculated from their primary sequences (ε = 820,000 $M^{-1}{\cdot}cm^{-1}$; molecular mass, 723 kDa). The purified dynein complex was supplemented with glycerol to a final concentration of 20% (vol/vol), flash-frozen in small aliquots, and stored in liquid nitrogen. The final yield of the purified dynein complex was ~0.2–0.3 mg of protein, with a final concentration of ~0.2 mg/mL.

To test the role of different accessory subunits in dynein heavy-chain assembly, we purified cytoplasmic dynein subcomplexes with different subunit combinations by leaving out one or more accessory subunits during the reconstitution and purification protocol. The protein concentration that could be reached with these purified subcomplexes was determined from the SYPRO Ruby–stained SDS gel-band intensities of their heavy chain using purified complex as a calibration standard. This allowed comparison of the solubility of these partial complexes with the complete complex.

For purification of the dynein complex under higher-ionic-strength conditions, lysis buffer B, elution buffer B, and gel-filtration buffer B were used.

Tubulin purification and labeling. Pig brain tubulin was purified as described previously (3) and labeled with Alexa Fluor 568 *N*-hydroxysuccinimide (NHS) (Invitrogen) or biotin–NHS (Thermo Fisher Scientific) (4). Tubulin concentrations refer to dimers.

Antibody production. Polyclonal antibody against cytoplasmic dynein light chain RB1 (α-RB1 antibody) was generated by immunizing rabbits (Eurogentec) with the purified recombinant RB1. Rabbit antiserum was purified by antigen-specific affinity chromatography using purified RB1 covalently coupled to HiTrap NHS-activated HP column (GE Healthcare) following standard procedures. The antibody concentration was determined by Bradford using BSA as a standard, and the purity was analyzed by SDS/PAGE. Purified polyclonal antibody was stored in small aliquots at –20 °C in PBS containing 50% (vol/vol) glycerol.

Other proteins. Monomeric and dimeric kinesin–mGFP containing either the first 340 (Kin340-mGFP) or 401 (Kin401-mGFP) amino acids of the *Drosophila melanogaster* kinesin-1 heavy chain, respectively, fused to mGFP were expressed and purified as described previously (5, 6).

Sedimentation-Velocity Analytical Ultracentrifugation. Sedimentation-velocity ultracentrifugation was used to determine the sedimentation coefficients of dynein constructs. For sedimentation-velocity runs in standard buffer conditions, proteins were purified by IMAC (as described above) using lysis buffer A and elution buffer A and then gel-filtered into analytical ultracentrifugation (AUC) buffer A [30 mM Hepes, 150 mM KOAc, 2 mM $MgSO_4$, 0.68 M glycerol, 2 μM Mg-ATP, 0.2 mM TCEP (Tris(2-carboxyethyl)phosphine; Sigma) (pH 7.0)]. For measuring the sedimentation coefficients under higher-ionic-strength conditions (Fig. S4*B*), proteins were purified by IMAC using lysis buffer B and elution buffer B and then gel-filtered into AUC buffer B [20 mM KH_2PO_4, 250 mM KCl, 2 mM $MgCl_2$, 0.68 M glycerol, 2 μM Mg-ATP, 0.2 mM TCEP (pH 7.2)]. For each sedimentation-velocity run, 400 μL of protein sample was analyzed. The dynein complex, CDHC-IC-LIC, and CDHC were prepared at ~200 nM concentrations and CDHC-LIC at ~100 nM, whereas Dyn380kD

and cc-Dyn380kD were analyzed at concentrations ranging from 300 nM to 1.2 μM.

Sedimentation-velocity ultracentrifugation was performed in a Beckman analytical ultracentrifuge (model Optima XLA) equipped with an UV-absorption optical system and an An-Ti50 rotor. Experiments were done in double-sector charcoal-Epon cells at 20 °C at 30,000 or 40,000 rpm. Scans of absorbance at 230 or 280 nm were recorded using a spacing of 0.003 cm in a continuous scan mode. Absorbance scans were taken at 230 nm when the concentration of the sample was lower than 400 nM; otherwise, the scans were collected at 280 nm. Data were analyzed with DCDT+ (Version 2.3.2), using the refined version of time-derivative method (7). The density and viscosity of each sample buffer and the partial specific volume of each protein were calculated using SEDNTERP (Version 1.09). The Gaussian function was fitted to sedimentation coefficient distributions to obtain the sedimentation coefficients of each protein species.

Analytical Gel Filtration. Stokes radii of dynein constructs were measured by gel-filtration chromatography using a Superose 6 PC 3.2/30 column (GE Healthcare) equilibrated in AUC buffer A and using protein standards of known Stokes radii for calibration [Gel Filtration Calibration Kits LMW and HMW (GE Healthcare): thyroglobulin (8.5 nm), ferritin (6.1 nm), aldolase (4.81 nm), ovalbumin (3.05 nm), and ribonuclease A (1.64 nm)]. Dynein constructs were prepared as described for analytical ultracentrifugation experiments. For each gel-filtration experiment, 50 μL of protein sample was analyzed. Elution volumes (V_e) were measured by fitting a Gaussian function to the elution peaks using OriginPro (Version 8.6). The elution volume parameter K_{av} was calculated for each protein using

$$K_{av} = \frac{V_e - V_0}{V_c - V_0}$$

where V_c is the geometric column volume (2.4 mL for a Superose 6 PC 3.2/30), and V_0 is the column void volume (determined from the elution volume of Blue Dextran 2000). The calibration curve

$$\sqrt{-\log(K_{av})} = a*R_s + b$$

was used to calculate the Stokes radii (R_s) of the dynein constructs.

For measuring Stokes radii under higher-ionic-strength conditions (Fig. S4*C*), analytical gel filtration was carried out as described above, but both the protein standards and dynein constructs were separated on a column equilibrated with AUC buffer B.

Molecular Mass Determination. The molecular masses of dynein constructs were calculated using the experimentally determined Stokes radii and sedimentation coefficients using the Svedberg equation:

$$M = \frac{6\pi * \eta * N * R_s * s}{1 - \nu * \rho}$$

where M is molecular mass, η is viscosity of the water at 20 °C (0.01 $g{\cdot}cm^{-1}{\cdot}s^{-1}$), N is Avogadro's number (6.022×10^{23}), R_s is Stokes radius of the protein (nanometers), s is a sedimentation coefficient of the protein corrected to standard conditions [at 20 °C in water: s(20,w); 10^{-13} s (S)], ν is partial specific volume of the protein (cubic centimeter per gram), and ρ is density of the water at 20 °C (1 $g{\cdot}cm^{-3}$).

Subunit Stoichiometry Determination in the Reconstituted Dynein Complex. Five out of six subunits in the purified dynein complex were analyzed by quantifying their band intensities of SYPRO Ruby–stained (Molecular Probes) SDS gels using protein standards of known concentration for calibration. The amount of dynein heavy chain (CDHC; 560 kDa per monomer) and dynein IC (IC1; 71 kDa) in the complex was estimated using Dyn380kD (413 kDa) and BSA (Sigma; 69 kDa), respectively, of known concentration as a standard. The amount of LIC (LIC2; 54 kDa) and two light chains [RB1 (11 kDa) and Tctex1 (13 kDa)] in the complex was estimated using the purified proteins of known concentration as a standard. The SYPRO Ruby–stained SDS gels were scanned [with a range of exposure times (0.25–4 s), depending on the subunit analyzed] using ImageQuant LAS 4010 (GE Healthcare), and the intensity of the bands of each protein was determined using ImageQuantTL software. Subunit stoichiometry is presented as a ratio of calculated amounts of individual subunits.

Because the LC8 light chain was not well separated by SDS/PAGE from RB1 and was not well stained with SYPRO Ruby, LC8 and RB1 were also quantified by Western blotting, using purified proteins of known concentration as a standard. We determined the ratio of LC8 and RB1 light chains per LIC2 in the dynein complex, by quantifying LIC2 from the same gel using SYPRO Ruby for staining. In detail, serial dilutions of standards (purified LIC2, LC8, and RB1) and purified dynein complex were run on an SDS gel. The gel was then cut horizontally at the 25-kDa marker. The upper part of the gel was stained with SYPRO Ruby gel stain, and the amount of LIC2 was quantified as described above. The lower part of the gel was wet-blotted on a nitrocellulose membrane with 0.1-μm pore size (Whatman), and the blot was blocked using Odyssey blocking buffer (Licor). LC8 was detected using polyclonal rabbit α-LC8 antibody (ab87283; Abcam), and RB1 was detected using α-RB1 antibody. The primary antibodies were detected using IR secondary antibody (IRDye 680LT goat anti-rabbit IgG; Licor), and the blots were scanned and analyzed using Licor Odyssey Infra-red Imager.

Negative-Staining EM. Purified dynein constructs were diluted in 30 mM Hepes, 150 mM KOAc, 2 mM $MgSO_4$, 0.1 mM ATP, and 10 β-mercaptoethanol (pH 7.2) at ∼3 nM final concentration. A total of 4 μL of the sample solution was applied to a carbon-coated grid (Plano), previously activated by glow discharge. After 2 min, the grid was washed quickly three times with water and four times with 2% uranyl acetate (wt/vol), blotting the liquid away after each step and leaving the grid to air-dry after the last step. Samples were imaged with a Tecnai G2 Spirit Twin transmission electron microscope (FEI Company) at a voltage of 120 kV and an Ultrascan CCD (Gatan). The diameter of dynein motor domains and the length of the dynein complex tail were measured using ImageJ.

MT-Gliding Assays. ***MT-gliding assay on Tris-Ni-NTA surface.*** Tris-NTA-PEG–functionalized glass coverslips were prepared and loaded with nickel ions as described previously (8). Flow chambers were built from a Tris-Ni-NTA-PEG coverslip and poly(L-lysine) (PLL)-PEG–passivated counter glass, separated by two strips of double-sided sticky tape (Tesa). Taxol-stabilized and polarity-marked MTs were prepared as described previously (8, 9). The flow chamber was additionally passivated by incubation with 5% Pluronic F-127 in water (wt/vol) for 5 min and then placed on an ice-cold metal block and washed with immobilization buffer (gel-filtration buffer A). His_6–motor diluted in immobilization buffer at concentrations between 1 and 500 nM was incubated for 30 min. Unbound proteins were washed off with immobilization buffer, followed by washing with assay buffer (AB) [10 mM Pipes, 35 mM KOAc, 2 mM $MgSO_4$, 1 mM EGTA, 2 mM β-mercaptoethanol, 10 μM Taxol (pH 7.0)]. The flow chamber

was then allowed to warm up to room temperature, and AB supplemented with 2 mM Mg-ATP, oxygen scavenger system [20 mM glucose, 20 μg/mL catalase (Sigma), and 160 μg/mL glucose oxidase (Serva)], and 50–300 nM Alexa568-labeled MTs was flowed into the chamber. MTs were immediately visualized at 25 ± 1 °C by shuttered time-lapse TIRF microscopy [IX71 (Olympus); using a setup as described (6)], with a 60× objective. Samples were excited at 532 nm, and images were acquired at 1-s time intervals with 100-ms exposure times. For landing-rate experiments, five consecutive images of the sample (and of a control sample lacking motor) were also taken with 488-nm excitation and with 30- to 400-ms exposure time (depending on the concentration used for immobilization). Movies S2, S3, and S4 have been compressed to reduce file size.

MT-gliding assay on nonfunctionalized glass. Flow chambers were built from untreated glass coverslips and PLL-PEG–passivated counter glass. The flow chamber was passivated by incubation with 5% Pluronic F-127 in water (wt/vol) for 5 min and was washed with immobilization buffer. Dynein complex diluted in immobilization buffer at concentrations between 5 and 150 nM was flown in a chamber and incubated for 3 min, followed by 1 min of incubation with 5 mg/mL β-casein in immobilization buffer. Unbound proteins were washed off with immobilization buffer, followed by washing with AB and AB supplemented with 2 mM Mg-ATP, oxygen scavenger system (same as described above), and 50–300 nM Alexa568-labeled MTs were flown in the chamber, and MTs were immediately visualized in the same way as described above.

Kymograph analysis of gliding assays. To determine the velocities of MT gliding from a time-lapse movie, the tracks of gliding MTs were analyzed with the "Multiple Kymograph" plug-in for ImageJ (J. Rietdorf and A. Seitz, EMBL, Heidelberg, Germany). Velocities were determined from kymographs (time-space plots) for intervals of 1–2 min. Approximately 100 MTs were analyzed per condition. A Gaussian function was fitted to gliding velocity histograms using OriginPro. The reported mean velocity is the center of the peak of the fitted Gaussian function and the reported error is SD.

Landing-rate assay analysis. To determine the motor density on the surface, we measured the average background-corrected mGFP intensity from the images taken with 488-nm excitation. The exposure time was chosen to avoid signal saturation; the measured intensities were then normalized with exposure time after ensuring a linear dependence. Variations in excitation intensities on different days were corrected for by using fluorescent beads as calibration standards.

The landing rate for each motor density was calculated by measuring the number of MTs within a field of view (18,700 μm^2) that landed within 1–5 min (depending on motor density and MT concentration) and moved at least for three consecutive frames (corresponding to 0.8 μm). The landing rates were corrected for different MT concentrations after ensuring the rates depended linearly on the MT concentration. In the absence of immobilized motors, no MTs landed on the surface.

To quantify the minimal number n of motors required for MT transport, the dependence of the MT landing rate, Ln, was plotted as a function of the motor density, ρ, and the following function was fitted to the data, as previously described (10):

$$Ln(\rho) = A^{*}\left(1-e^{-\frac{\rho}{\rho_0}}\right)^{n}$$

The fit was performed using logarithmic values of landing rates. We confirmed that the determination of the minimal motor numbers required for MT transport was not affected by potential changes in the length distribution of the landing MTs with changing motor density.

Single-Molecule Imaging Assay. Individual mGFP-labeled motors were imaged at low concentrations on immobilized fluorescently labeled MTs using TIRF microscopy (8). Flow chambers were built from biotin–PEG–functionalized coverslips and PLL-PEG–passivated counter glass. The flow chamber was additionally passivated by incubation with 5% Pluronic F-127 in water (wt/vol) for 5 min on an ice-cold metal block, followed by washing with 50 μg/mL κ-casein (Sigma) in AB. To enable MT immobilization, 50 μg/mL κ-casein and 100 μg/mL NeutrAvidin (Invitrogen) in AB were incubated for 5 min, and the flow chamber was washed with 50 μg/mL κ-casein in AB. The flow chamber was then allowed to warm up to room temperature, and ∼40 nM biotinylated and Alexa568-labeled MTs in AB were flown into the chamber and incubated for 5 min. Nonbound MTs were washed out with AB, and, finally, AB containing a nucleotide [2 mM Mg-ATP, unless otherwise stated; or 1 mM Mg-AMP-PNP (Sigma)], oxygen scavenger system (20 mM glucose, 20 μg/mL catalase, and 160 μg/mL glucose oxidase), and mGFP–motor (at concentrations as indicated in the figure; typically 50–100 pM mGFP–dynein complex, 30–500 pM mGFP-Dyn380kD, or mGFP-cc-Dyn380kD, and 10 pM of Kin401-mGFP) was flowed into the chamber. Motors were immediately visualized by TIRF microscopy (100× objective; 1.6× optovar) and recorded by continuous streaming in the mGFP channel (488-nm excitation; 100-ms exposure time) for 70 s, followed by generation of a static image of MTs averaging a continuous stream of 10 images (532-nm excitation; 100-ms exposure time). The temperature was maintained at 25 ± 1 °C.

To determine the behavior of single fluorescent motors on the MTs in the recorded streams, kymographs along individual MTs were created using the Multiple Kymograph plug-in in ImageJ. Dwell times (total event duration) and, for Kin401-mGFP, the run length (travel distance) and mean velocity were determined from a manual analysis of the positions and times of motor landing on the MT and dissociation from it. The cutoff for event identification was 300 ms (an event had to be observed in at least three consecutive frames). Velocities of all Kin401-mGFP runs in a movie were displayed in a histogram to which a Gaussian function was fitted yielding the mean velocity at the center of the peak.

The number of events is given as a total number of events per minute divided by the concentration of motor and the total length of all MTs in the field of view.

To determine the mean dwell times of mGFP-Dyn380kD and mGFP-cc-Dyn380kD in the presence of AMP-PNP, we considered only completely observed binding events (events where both motor landing and motor dissociation occur within the duration of the movie). The percentage of the mGFP-Dyn380kD "complete" events was 90–95% of all events (for the rest of the events, either landing or dissociation was not detected, because it happened before the start or after the end of the movie, respectively), and the percentage of the mGFP-cc-Dyn380kD complete events was ∼80% of all events (for 15%, either landing or dissociation was not detected, and 5% were continuously bound from the beginning to the end of the movie). The cumulative distribution function (cdf) of data were calculated for the complete events using the "ecdf" function in Matlab (R2011b), and a monoexponential function was fitted to (1 – cdf) data using OriginPro:

$$1-cdf = A^{*}e^{\frac{t}{\tau}}$$

with amplitude (A), dwell time (t), and mean dwell time (τ). Reported errors are SEM.

GFP fluorescence intensity analysis of single molecules. To measure fluorescence intensities of single molecules, mGFP-fused motors at 40–80 pM concentration, diluted in AB supplemented with 2 mM Mg-ATP and oxygen scavenger system (20 mM glucose, 375 μg/mL glucose oxidase, 90 μg/mL catalase) were nonspecifically

adsorbed onto a glass surface and imaged by continuous streaming with either 400-ms exposure time for 20 s (Fig. S7*A*, *Upper*) or with 100-ms exposure time for 5 s (Fig. S7*A*, *Lower*) using TIRF microscopy. For the intensity distribution analysis, the raw image stack was imported into ImageJ, and the central two-thirds of each image was selected for analysis. The "GaussianFit" plug-in (http://valelab.ucsf.edu/~nico/IJplugins) was used to measure the integrated intensity of individual fluorescence signals, by fitting 2D Gaussian profiles to every molecule in each frame of the image stack. The fitting parameters and background were automatically calculated using 15 × 15 pixel regions around each molecule. The fitting results were imported into Origin 8.5 and were filtered to remove obviously spurious data, based on an estimated width of 220 nm for the optical point-spread function of the microscope. Relative frequency histograms of the integrated intensity were calculated; this was repeated for four to five different image stacks for each construct assayed, and the histograms were averaged.

1. Zacharias DA, Violin JD, Newton AC, Tsien RY (2002) Partitioning of lipid-modified monomeric GFPs into membrane microdomains of live cells. *Science* 296(5569): 913–916.
2. Fitzgerald DJ, et al. (2006) Protein complex expression by using multigene baculoviral vectors. *Nat Methods* 3(12):1021–1032.
3. Castoldi M, Popov AV (2003) Purification of brain tubulin through two cycles of polymerization-depolymerization in a high-molarity buffer. *Protein Expr Purif* 32(1): 83–88.
4. Hyman A, et al. (1991) Preparation of modified tubulins. *Methods Enzymol* 196: 478–485.
5. Bieling P, Telley IA, Piehler J, Surrey T (2008) Processive kinesins require loose mechanical coupling for efficient collective motility. *EMBO Rep* 9(11):1121–1127.
6. Telley IA, Bieling P, Surrey T (2009) Obstacles on the microtubule reduce the processivity of Kinesin-1 in a minimal in vitro system and in cell extract. *Biophys J* 96(8):3341–3353.
7. Philo JS (2006) Improved methods for fitting sedimentation coefficient distributions derived by time-derivative techniques. *Anal Biochem* 354(2):238–246.
8. Bieling P, Telley IA, Hentrich C, Piehler J, Surrey T (2010) Fluorescence microscopy assays on chemically functionalized surfaces for quantitative imaging of microtubule, motor, and +TIP dynamics. *Methods Cell Biol* 95:555–580.
9. Roostalu J, et al. (2011) Directional switching of the kinesin Cin8 through motor coupling. *Science* 332(6025):94–99.
10. Hancock WO, Howard J (1998) Processivity of the motor protein kinesin requires two heads. *J Cell Biol* 140(6):1395–1405.

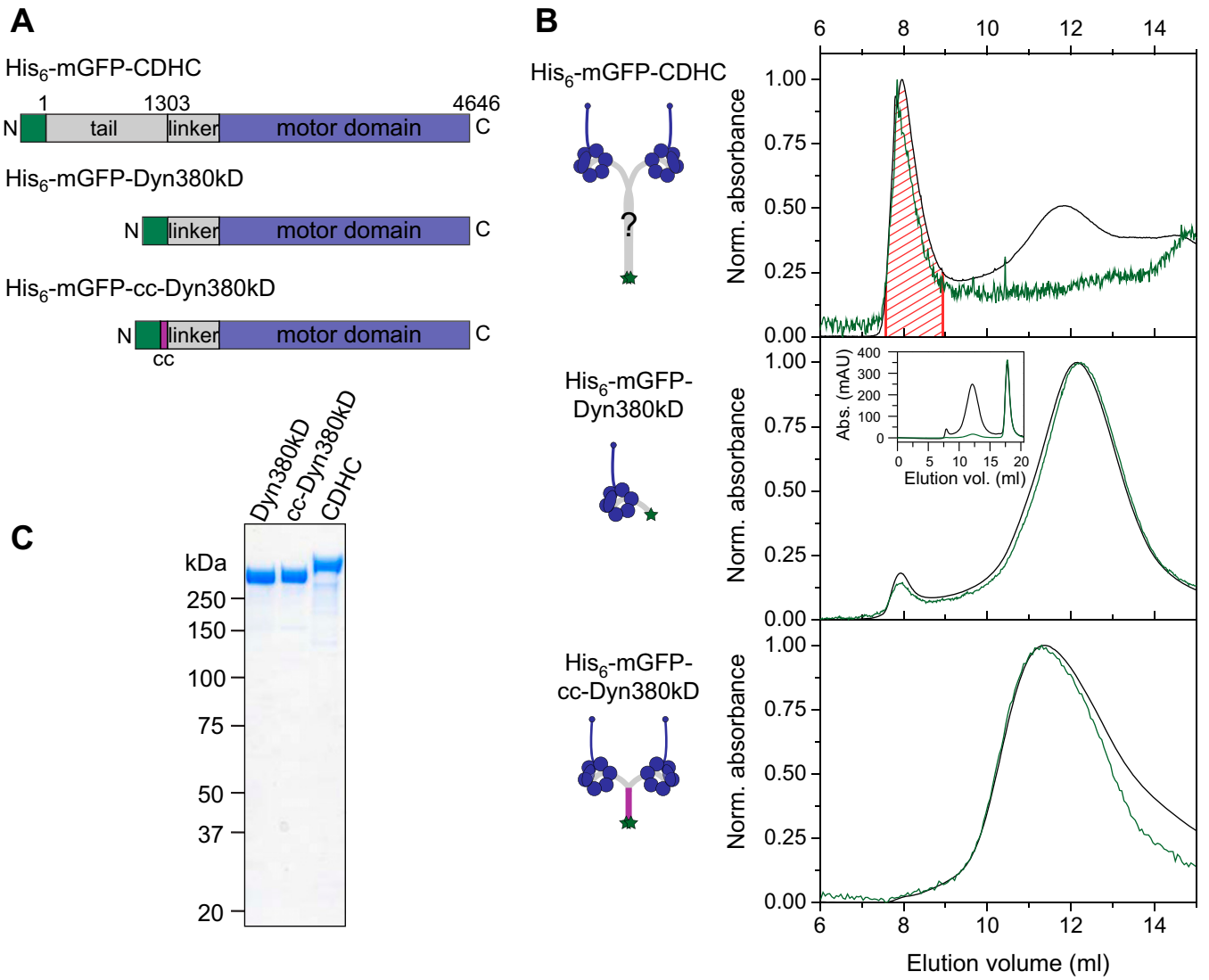

Fig. S1. Human cytoplasmic dynein heavy chain (CDHC) constructs used in this study. (*A*) Schematic of the domain organization of the dynein heavy-chain sequences used here. All constructs carry a N-terminal His_6 tag and a mGFP (green): full-length CDHC, monomeric cytoplasmic dynein motor domain (Dyn380kD), and artificially dimerized cytoplasmic dynein motor domains (cc-Dyn380kD), generated by fusion of kinesin-1 coiled coil (cc) to the N terminus of the dynein motor domain. (*B*) Preparative gel-filtration profiles of the three constructs with normalized absorbance values at 280 nm (black line) and 488 nm (green line) in the region around the dynein elution peaks. CDHC purified in the absence of its accessory subunits showed poor solubility throughout the purification and eluted in the void-volume peak, suggestive of protein aggregation. The collected CDHC fraction (red shaded area) was rather insoluble (Table 1). In contrast, truncated dynein constructs Dyn380kD and cc-Dyn380kD were highly soluble and eluted as a single peak after the void-volume peak during gel filtration, showing no signs of aggregation. This result strongly suggests that the tail domain of human CDHC is not sufficient for heavy-chain dimerization, but rather causes aggregation in the absence of the other subunits of the dynein complex. (*Inset*) Elution profile over an extended range. All preparations contained truncated mGFP that eluted after dynein and could be well separated. (*C*) Coomassie-stained SDS gel of purified Dyn380kD, cc-Dyn380kD, and CDHC.

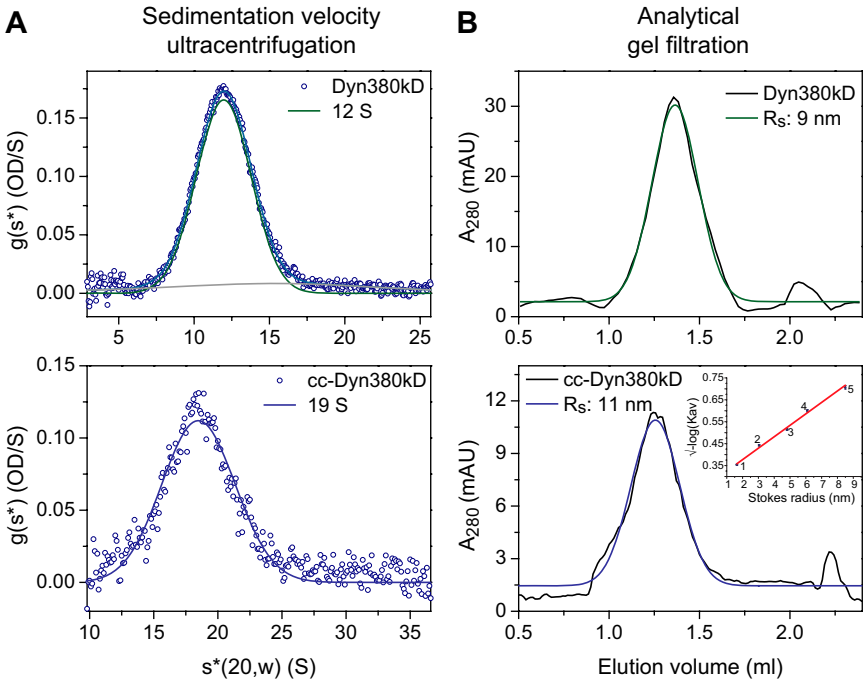

Fig. S2. Hydrodynamic properties of dynein motor domain Dyn380kD and artificially dimerized motor domains cc-Dyn380kD. This figure supplements Fig. 2 *A*–*C*. (*A*) Sedimentation coefficient distributions [g(s*) plots] of Dyn380kD (*Upper*) and cc-Dyn380kD (*Lower*) as obtained from analytical sedimentation-velocity ultracentrifugation. Gaussian fits (lines) to the data (blue circles), with the center being at 12S for the major species (85%) of Dyn380kD (green line) and 19S for the single species of cc-Dyn380kD (blue line). The gray and blue lines in the upper plot represent a minor population and the sum of two species of Dyn380kD, respectively. (*B*) Analytical gel-filtration profiles of Dyn380kD (*Upper*) and cc-Dyn380kD (*Lower*) with absorbance values at 280 nm. Gaussian fits (colored lines) to the data (black lines), with the center of the peak corresponding to K_{av} values of 0.26 for Dyn380kD (green line) and 0.18 for cc-Dyn380kD (blue line). Corresponding Stokes radii, R_s, are as indicated. (*Inset*) Gel-filtration calibration curve for the determination of Stokes radii. The plot shows $\sqrt{}$-log(K_{av}) values of protein standards as a function of the known Stokes radii (blue diamonds) and a linear fit (red line). Shown are SEM. 1, RNase A; 2, ovalbumin; 3, aldolase; 4, ferritin; 5, thyroglobulin. Adjusted R^2 = 0.992.

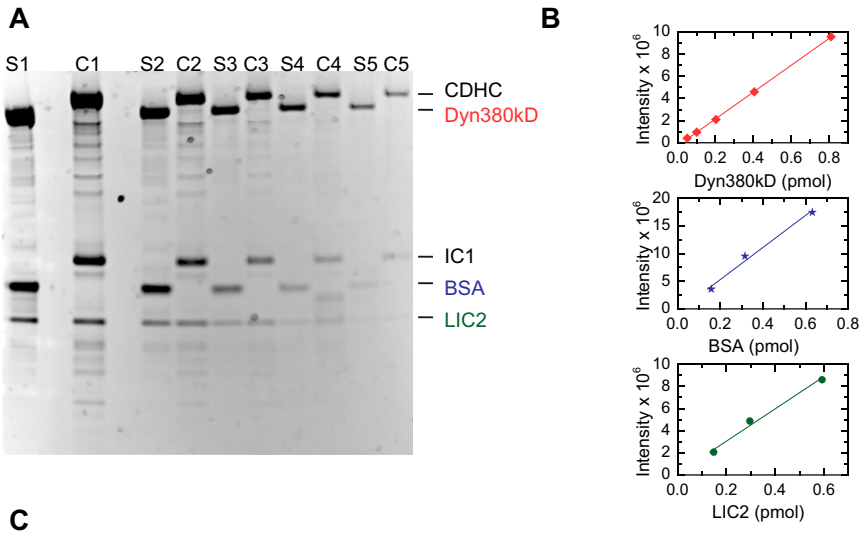

C

Subunit stoichiometry					
lane	CDHC (pmol)	IC1 (pmol)	LIC2 (pmol)	CDHC:IC1	CDHC:LIC2
C1	0.561	0.436	0.635	1.29:1	1:1.13
C2	0.245	0.228	0.303	1.08:1	1:1.24
C3	0.116	0.119	nd	1:1.03	nd

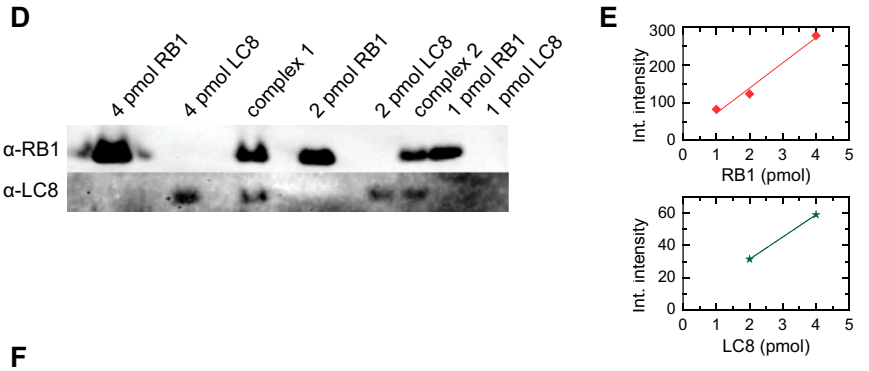

F

Subunit stoichiometry					
lane	LIC2 (pmol)	RB1 (pmol)	LC8 (pmol)	LIC2:RB1	LIC2:LC8
complex1	1.80	0.99	2.19	1.8:1	1:1.2
complex2	0.85	0.55	1.24	1.6:1	1:1.5

Fig. S3. Quantification of the subunit stoichiometry in the reconstituted dynein complex. This figure supplements Fig. 2*D*. (*A*) SYPRO Ruby–stained SDS gel with serial dilutions of a mixture of calibration proteins [Dyn380kD, BSA, and LIC2 (S1–S5) at known concentrations] and of the reconstituted dynein complex (C1–C5; with CDHC, IC1, and LIC2 labeled). (*B*) Calibration curves of gel-band intensities of Dyn380kD (red), BSA (blue), and LIC2 (green) (as measured in the calibration protein mixtures S1–S5 in *A*) as a function of the protein amounts loaded per lane. (*C*) Table showing the amounts of the subunits in the dynein complex (as detected in *A* and calculated using the calibration curves shown in *B*) and the corresponding molar ratio of subunits. Note: smaller subunits were below the detection limit in lanes S4 and S5 and C4 and C5. (*D*) Western blot with serial dilution of RB1 and LC8 light chains of known concentrations and of the dynein complex (probed against RB1 and LC8 light chains). (*E*) Calibration curves of Western blot band intensities of the purified protein standards (RB1 in red, LC8 in green) as a function of protein amounts loaded per lane. (*F*) Table with the determined amounts of subunits in the dynein complex and the corresponding molar ratio of subunits. RB1 and LC8 amounts were calculated using the calibration curves shown in *E*, and the amounts of LIC2 were calculated from the SYPRO Ruby–stained upper part of the SDS gel that was not used for blotting, using the LIC2 calibration curve (as shown in *A*–*C*).

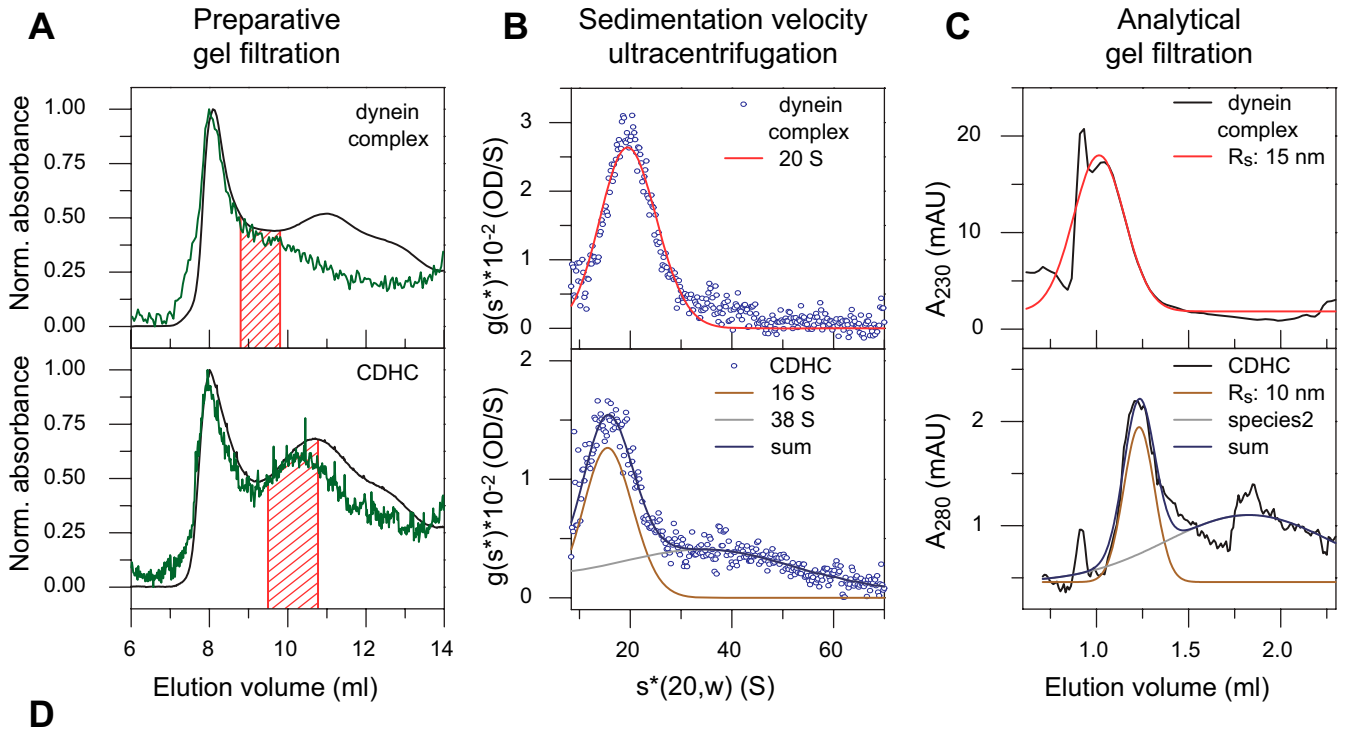

D

Oligomerization state of dynein constructs in high ionic strength buffer							
Protein	s(20,w) (S)	Stokes radius (nm)	part. spec. volume (ml/g)	calculated Mw (*10^3)	theoretical Mw (*10^3)	ratio	oligomerization state
dynein complex	20.0	15.0	0.737	1294	723	1.8	HC dimer
CDHC	16.1	10.1	0.739	705	563	1.25	monomer
Dyn380kD	11.9	7.6	0.738	394	413	0.95	monomer
cc-Dyn380kD	18.2	9.8	0.738	775	423	1.8	dimer

Fig. S4. Purification and oligomerization state of dynein constructs in higher-ionic-strength conditions. Dynein constructs in this experiment were both purified and analyzed in high-ionic-strength buffer (*SI Materials and Methods*). (*A*) Preparative gel-filtration profiles of the dynein complex (*Upper*) and the CDHC (*Lower*) in high-ionic-strength buffers showing normalized absorbance values at 280 nm (black line) and 488 nm (green line). Purifying CDHC under these conditions resulted in the appearance of a second CDHC peak (in addition to the void-volume peak) compared with standard conditions (Fig. S1*B*, *Top*). Red lines indicate the fractions that were collected and further analyzed by sedimentation-velocity ultracentrifugation (*B*) and analytical gel filtration (*C*). (*B*) Analytical ultracentrifugation: sedimentation coefficient distributions [g(s*) plots] of the dynein complex (*Upper*) and the CDHC (*Lower*) in high-ionic-strength buffer. Gaussian fits (lines) to the data (blue circles) with the center at 20S for the dynein complex (red line), 16S for the lower s-value species of CDHC (brown line; 46%), and 38S for the higher s-value species (gray line; 54%). These results show that even under these conditions, the CDHC sample is more heterogeneous than the dynein complex. (*C*) Analytical gel-filtration profiles of the dynein complex (*Upper*) and the CDHC (*Lower*) (with absorbance values as indicated). Gaussian fits (colored lines) to the data (black lines) with the center of the peak corresponding to a K_{av} value of 0.08 for the dynein complex (red line) and 0.23 for the main eluate of the CDHC (brown). Stokes radii, R_s, are as indicated. For comparison: the K_{av} values for cc-Dyn380kD and Dyn380kD under the same conditions were 0.25 and 0.34, respectively. (*D*) Summary of results from the analytical sedimentation-velocity ultracentrifugation [s(20,w)] and analytical gel filtration (Stokes radius). The oligomerization state was determined as the ratio of the molecular mass (Mw) as calculated from the experimental values and the theoretically expected molecular mass of a monomer. These results show that the CDHC purified in the absence of its accessory subunits forms either monomers or high oligomers and aggregates. In contrast to CDHC alone, the dynein complex existed as a single species under these conditions, consistent with containing a heavy-chain dimer.

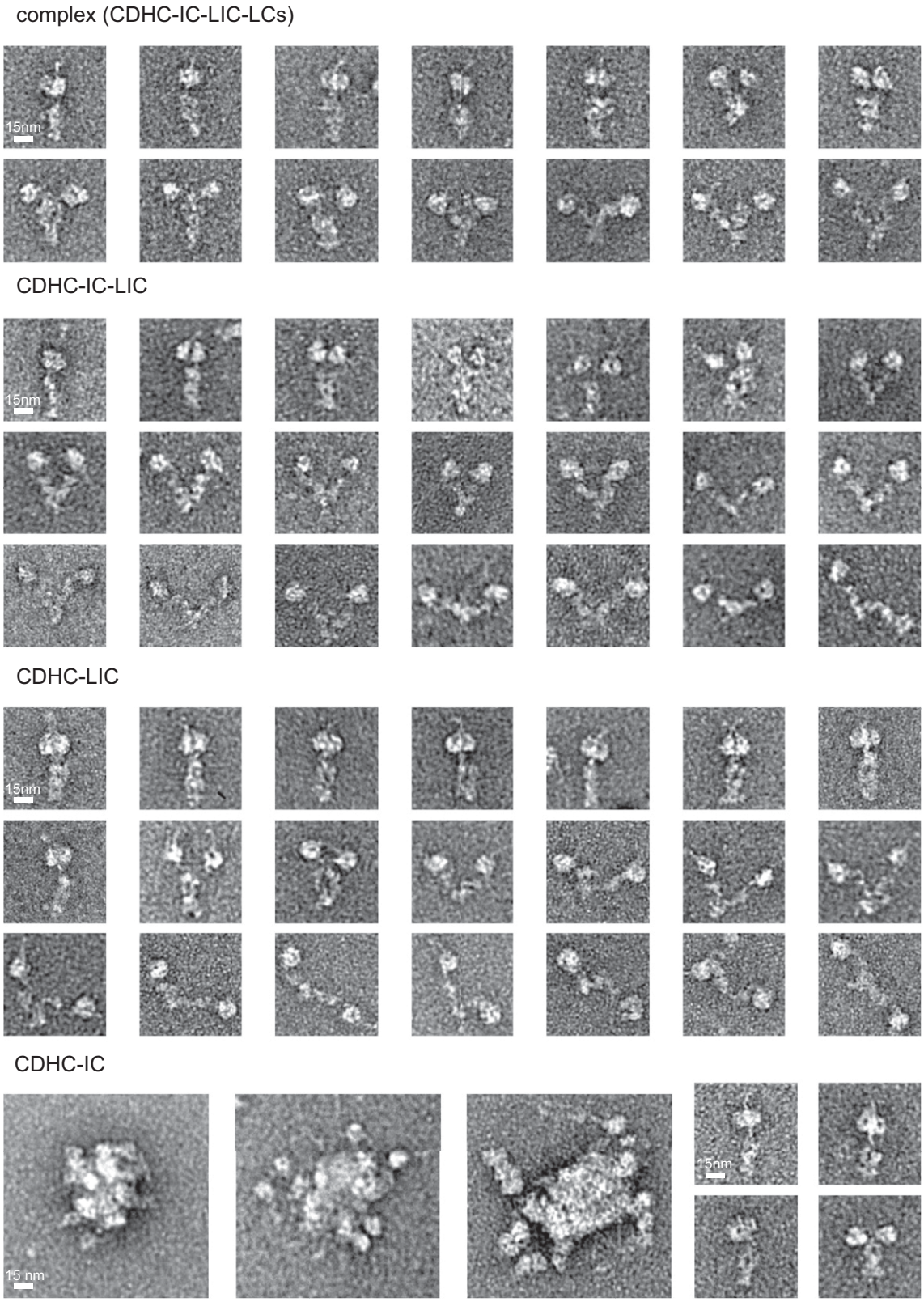

Fig. S5. EM images of different negatively stained dynein subcomplexes. Galleries of single particles of the entire dynein complex and CDHC-IC-LIC, CDHC-LIC, and CDHC-IC preparations. Each image shows an area of 80 × 80 nm, except the larger images of heavy chain (HC)-IC aggregates that show 160 × 160 nm area. These results confirmed that CDHC-IC is mostly aggregated (containing only few dimers) and showed that the combinations CDHC-IC-LIC and CDHC-LIC formed mostly complexes containing dimers of the heavy chain with the tail sometimes appearing less compact.

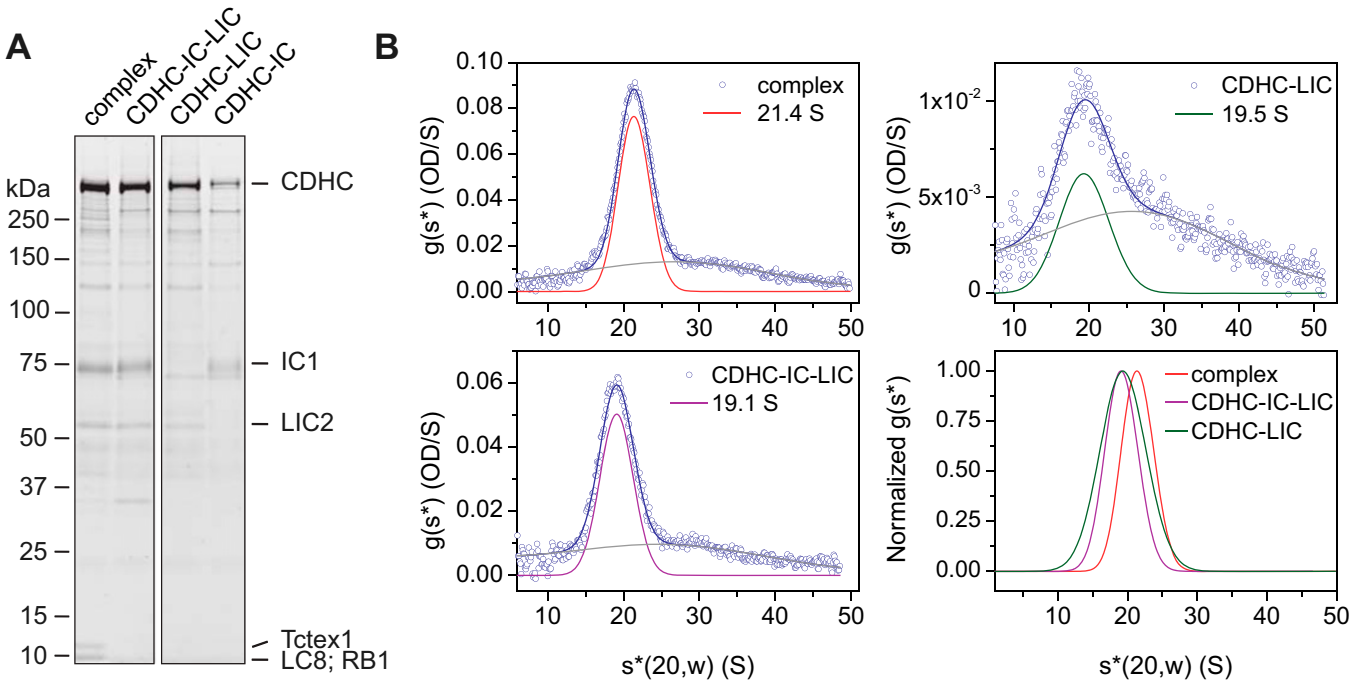

Fig. S6. Purification and hydrodynamic properties of the dynein heavy chain in combination with different sets of accessory subunits. This figure supplements Table 1. (*A*) SYPRO Ruby–stained SDS gel of the dynein heavy chain copurified with different subunit combinations. (*B*) Analytical ultracentrifugation: sedimentation coefficient distributions of the entire dynein complex and the combinations CDHC-IC-LIC and CDHC-LIC. The lines are Gaussian fits to the data (blue circles), with the center of the main peaks being indicated in the figure. For comparison, an overlay of the three normalized fits is shown (*Lower Right*). These results show that the s values of CDHC-IC-LIC and CDHC-LIC are similar to the s value of the entire dynein complex but are significantly lower. Given that the molecular mass of CDHC-IC-LIC is very similar to that of the complete complex, the lower s value indicates that the complex lacking the light chains is more elongated than the complete complex, suggesting that the tail is less compact than in the complete complex.

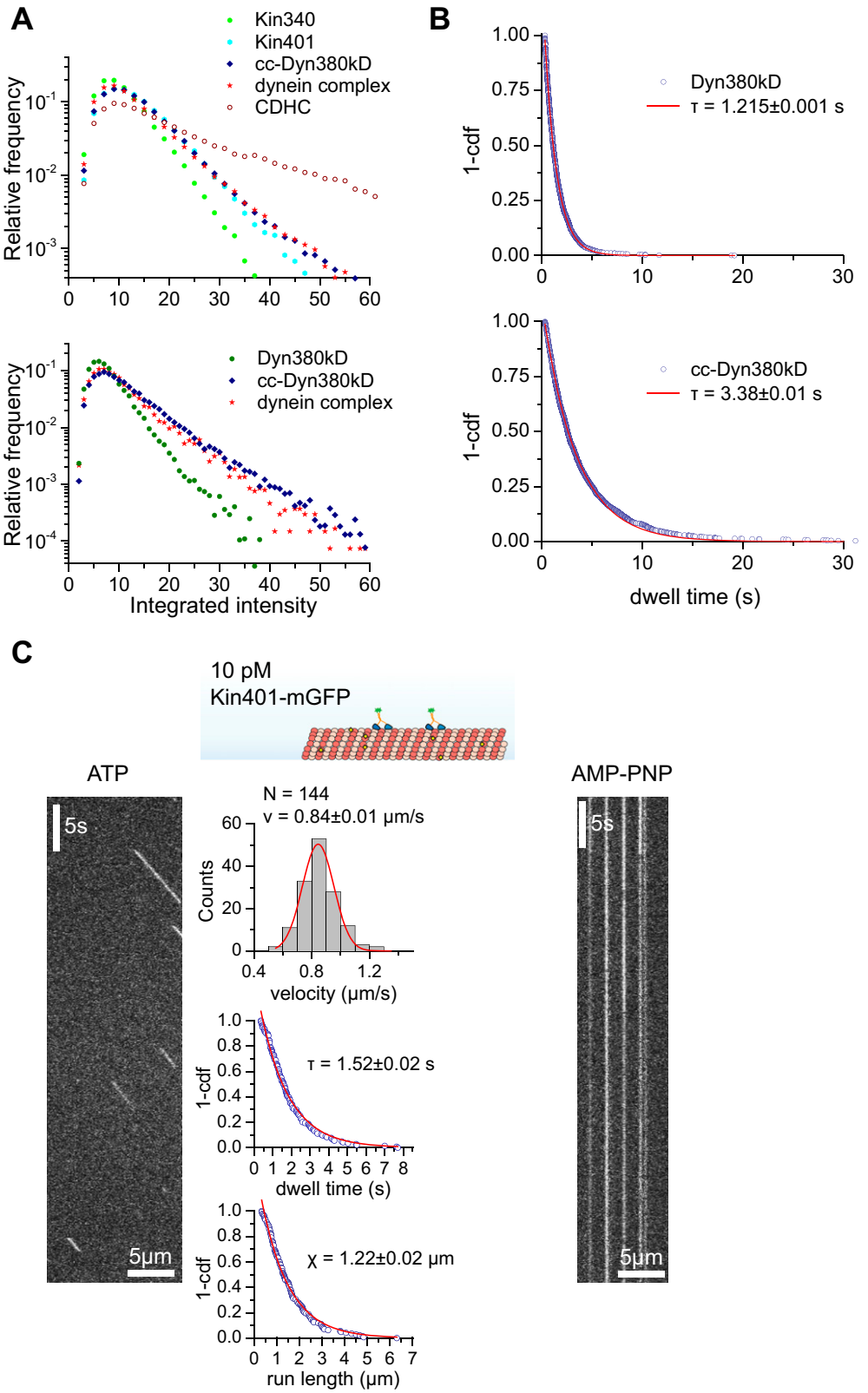

Fig. S7. Single-molecule TIRF microscopy data. (*A*) Single-molecule GFP fluorescence intensity distributions of *Drosophila* kinesin-1 constructs [monomeric Kin340-mGFP (light green circles) and dimeric Kin401-mGFP (cyan hexagons)] and dynein constructs [mGFP-Dyn380kD (green circles), mGFP-cc-Dyn380kD (blue diamonds), mGFP-dynein complex (red stars), and mGFP-CDHC (brown open circles)] presented as relative frequency. These data demonstrate that the dynein complex forms mostly dimers under single-molecule imaging conditions, similar to the artificially dimerized dynein motor domains (cc-Dyn380kD) and the kinesin-1 dimer (Kin401), in contrast to the monomeric kinesin (Kin340) and dynein motor domains (Dyn380kD). The dynein heavy chain alone forms a heterogeneous mixture including higher aggregates. (*B*) Dwell-time distributions (shown as 1 – cdf) of single mGFP-Dyn380kD (*Upper*, blue dots) and mGFP-cc-

Legend continued on following page

Dyn380kD (*Lower*, blue dots) molecules in the presence of AMP-PNP and a monoexponential fit (red lines), with mean dwell times of 1.215 ± 0.001 and 3.38 ± 0.01 s, respectively. Shown are SEM. The number of analyzed events was 1,290 and 1,071, respectively. Only interactions with clearly detectable binding and unbinding time points within the 70-s movie were analyzed. The longer dwell time of the dimeric construct in comparison with the monomeric motor domain is in agreement with the dimeric versus monomeric nature of the two constructs. (*C*) Single-molecule behavior of dimeric kinesin Kin401-mGFP on MTs imaged using TIRF microscopy, measured for control purposes. Exemplary kymographs showing individual Kin401-mGFP molecules interacting with MTs in the presence of 2 mM ATP or 1 mM AMP-PNP, as indicated. The concentration of Kin401-mGFP was 10 pM, and the temperature was 25 ± 1 °C. Individual Kin401-mGFP molecules moved processively along a MT in the presence of ATP. Histogram shows single Kin401-mGFP molecule velocity distribution with a Gaussian fit (red line), with a mean of 0.84 ± 0.01 μm/s. Run-length distribution and dwell-time distribution (shown as 1 – cdf) of single Kin401-mGFP molecules in the presence of ATP (blue dots) and a monoexponential fit (red line), yielding a mean run length of 1.22 ± 0.02 μm and a mean dwell time of 1.52 ± 0.02 s. Shown are SEM. The number N of analyzed events as indicated. In the presence of AMP-PNP, kinesin bound statically to MTs often for many tens of seconds.

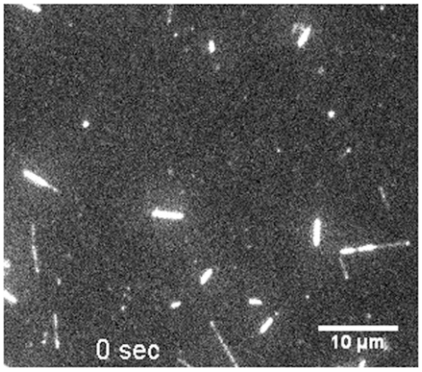

Movie S1. Polarity-marked MT gliding driven by the dynein complex immobilized on a Tris-Ni-NTA-PEG surface in the presence of ATP.

Movie S1

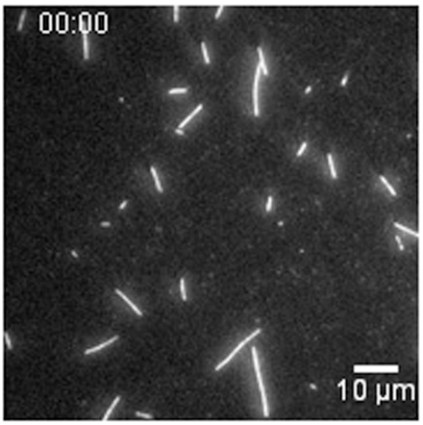

Movie S2. MT gliding driven by monomeric dynein motor domain (Dyn380kD) immobilized on a Tris-Ni-NTA-PEG surface in the presence of ATP.

Movie S2

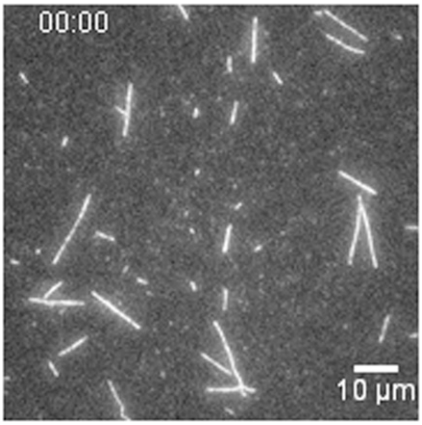

Movie S3. MT gliding driven by artificially dimerized dynein motor domains (cc-Dyn380kD) immobilized on a Tris-Ni-NTA-PEG surface in the presence of ATP.

Movie S3

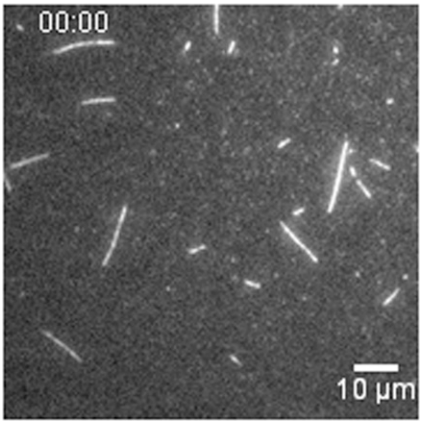

Movie S4. MT gliding driven by the dynein complex nonspecifically adsorbed on a nonfunctionalized glass in the presence of ATP.

Movie S4